Master's Thesis of Engineering

Aerial and Aquatic Applications of Ionic Polymer-Metal Composite

이온성 폴리머-금속 복합체의
공중과 수중에서의 적용

February 2023

Graduate School of Engineering
Seoul National University
Mechanical Engineering Major

Yejin Yu

Aerial and Aquatic Applications of Ionic Polymer–Metal Composite

Sung–Hoon Ahn

Submitting a master's thesis of
Mechanical Engineering

October 2022

Graduate School of Engineering
Seoul National University
Mechanical Engineering Major

Yejin Yu

Confirming the master's thesis written by
Yejin Yu
December 2022

Chair	Yong–Lae Park	(Seal)
Vice Chair	Sung–Hoon Ahn	(Seal)
Examiner	Kyungwon Han	(Seal)

Abstract

IPMC (Ionic Polymer-Metal Composite) is a synthetic polymer that is light-weight, and can be driven with low voltage. However, it has high hysteresis and weak driving force. This research sought to operate the system in which the conventional motor-driven system is not appropriate using IPMC. Problems were defined in aerial and aquatic environments, and methods for IPMC utilization were studied according to each application.

For aerial application, glider with control surfaces actuated by IPMC was designed and fabricated. Light-weight and low voltage drivable characteristics of IPMC could be efficiently utilized for the application. Hinge-type IPMC was selected to actuate control surfaces, and the control surfaces effectively change the trajectory of the glider.

For aquatic application, diaphragm pump whose diaphragm is actuated by IPMC was designed and fabricated. Biocompatibility and surface actuation characteristics of IPMC were applied in the system. Shape of IPMC constituting the diaphragm was selected to maximize the force, and sealing method to reduce hysteresis was developed.

Appropriate actuation and packaging method were developed to efficiently apply IPMC to each application.

Keyword: Ionic polymer-metal composite actuator, control surface, diaphragm pump

Student Number: 2021-28477

Table of Contents

Chapter 1. Introduction

1.1. Background

When designing a mechanical system, there are various methods to select an actuator to power the system. An electric motor driven system is commonly used for its high power and high robustness. However, this conventional motor driving method is not suitable in some applications. For example, some applications take weight to power ratio into consideration. Also, some applications require motion that activates in various forms other than rotational or translational motion. Conventional motor driven systems solve these problems with gear systems or with various motor combinations. However, gear systems often result in unpredictable frictions, and motor combinations often bring a lot into consideration. In addition, various applications require bio-compatibility, compact form factor, etc., and there are cases where the conventional motor system is not the best solution.

Ionic Polymer-Metal Composite (IPMC), first presented by Shaninpoor in 1998, has considerable complements when used as an actuator. IPMC is a synthetic composite that has electrode attached on a perfluorinated ionic polymer's surface. When electric field is applied, hydrated cations moves towards the cathode, which results in pressure distribution due to thickness difference, and shows bending in specific directions. This characteristic of IPMC allows it to be used as an actuator. Also, biocompatibility and low−voltage drivability (under 7 V) of IPMC further expand its usability. However, there remains limitations of IPMC as an actuator. Apart from complexity of IPMC fabrication and its low tip force, high hysteresis is one great limitation of IPMC. Since common IPMCs actuate using moisture on the surface as a medium, they lack stability and have short actuation life. Also, low tip force of the IPMC often makes it difficult to be used in macroscale systems.

In this study, IPMC were used in two applications, presenting simple fabrication and packaging methods that can show possibility of utilizing IPMC in various situations by reducing high hysteresis of IPMC and by finding the most force−efficient design.

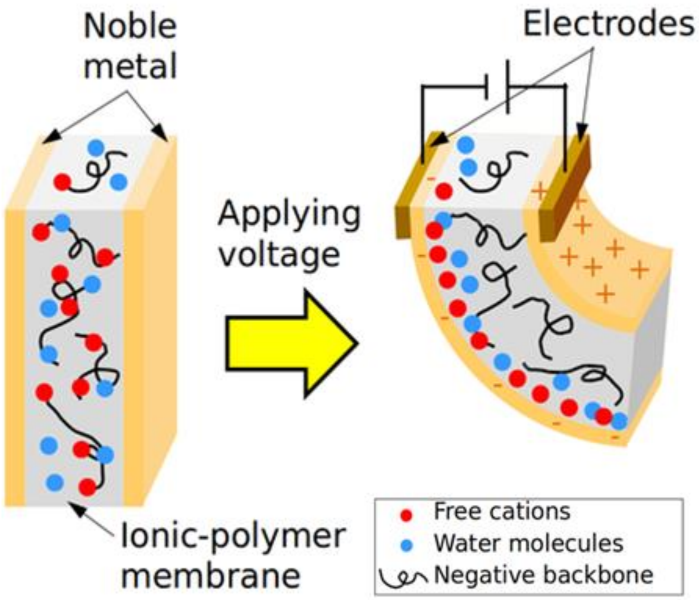

Figure 1.1 Actuation principle of IPMC

1.2. Outline of the Research

In this study, two problems were defined in aerial and aquatic environments. In the aerial environment, a glider was designed and fabricated to be controlled in desired direction. In the aquatic environment, a pump was designed and fabricated to transport fluid. Considering the specific environmental requirements (lightness in aerials and fluid transport pattern in aquatics), IPMC was used as an actuator instead of a conventional electric motor.

Chapter 2 briefly explains the characteristics and principle of the IPMC actuation along with the modeling of the IPMC actuation, and the method used to fabricate IPMC used in this study. Chapter 3 introduces the IPMC application on glider control surface actuation. Control surface mechanism is explained and the flight experiment is conducted. Chapter 4 introduces the novel design of diaphragm pump with its design, fabrication method, and evaluation. Finally, Chapter 5 concludes the two applications of IPMC.

Chapter 2. Fabrication and Evaluation of IPMC

2.1. Fabrication of IPMC

IPMC used in this study was made with Nafion 1110 as base polymer, platinum compound (Tetraammineplatinum (Ⅱ) chloride hydrate) for electrode, $NaBH_4$ for reducing agent, and NH_4OH as catalyst. IPMC fabrication method used in this study is as follows. Six IPMC sheets of 50 mm x 100 mm were produced in the following method.

① Roughen Nafion with sandpaper (600 grit)

② Cleanse roughened Nafion in 70°C distilled water for 15 minutes

③ Soak Nafion in 500 mL distilled water with 0.5 g platinum compound

④ Soak Nafion in 60°C 1.75 L distilled water with 2 g $NaBH_4$ for 1 hour

⑤ During step ④, add 0.5 g of $NaBH_4$ and 3 mL of NH_4OH every 15 minutes

⑥ Cleanse Nafion in 70°C distilled water for 5 minutes

⑦ Repeat ③−⑥ 4 times

⑧ Soak fabricated IPMC in NaOH for 3 days

Fabricated IPMC showed surface resistance of below 40 Ω.

2.2. Evaluation of IPMC Actuation

In order to confirm actuation properties of the fabricated IPMC, ANSYS simulation and actuation test were performed. ANSYS parameters were adjusted using the actual IPMC deformation test.

For both ANSYS simulation and actuation test, 10 mm x 50 mm beam−shaped IPMCs were prepared, with electrodes attached and clamped within 10 mm. The tip deformation of the IPMC after 50 seconds under constant voltage was assumed.

2.2.1 ANSYS Simulation

The properties of IPMC were set as Table 2.1. ANSYS simulation was conducted to find electro−mechanical coupling and thermal mechanical coefficients. The Young's modulus used in the simulation is obtained as follows:

$$E_b = \frac{1}{I}\left(\frac{2\pi}{3.515}\right)^2 f_n^2 m l^3 = \left(\frac{2\pi}{3.515}\right)^2 f_n^2 m l^3 \frac{12}{h t_\omega^3} \qquad \text{Eq. 2.1}$$

2.2.2 Actuation Test

IPMCs were driven under 1.5 V, 3.0 V, and 5.0 V under the clamping and duration conditions, same as the simulation. More than two IPMC pieces from the same fabrication batch were used to measure tip deformations. Real IPMCs had a 33% difference in activation ranges between front and back due to its hysteresis. To compare with the simulation, the average value was used.

Table 2.1 Parameters used in ANSYS simulation

Mass (m)	0.69 g
Length (l)	20 mm
Thickness (t_w)	254 μm
Inherent frequency (f_n)	0.6
Density	3387 kg/m^3
E	137 MPa
Coefficient of thermal expansion	0.0355

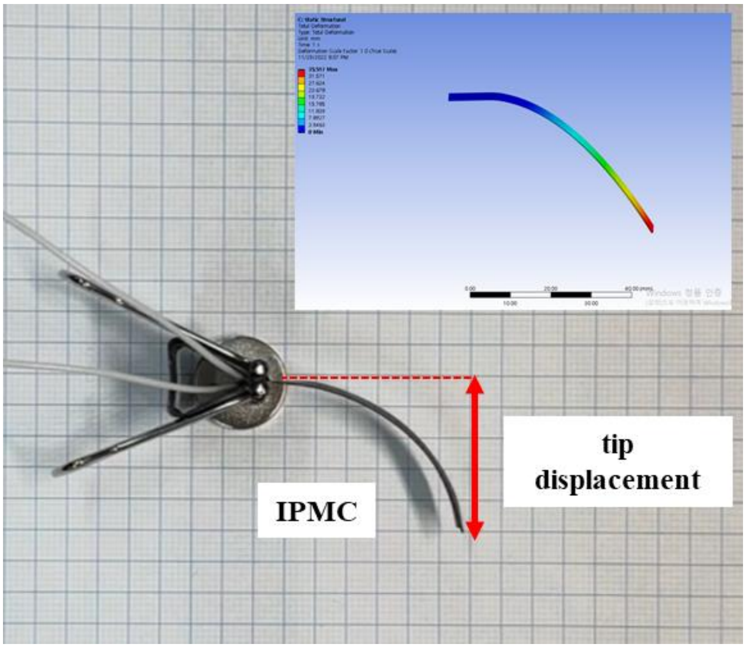

Figure 2.1 Simulation result and experimental result of IPMC actuation test

2.2.3 Results

The results obtained through each method are summarized in Table 2.2. It was confirmed that the parameters selected showed error rates of less than 8% under each voltage. In addition, the tip forces of the IPMC predicted by these parameters are shown. By using these simulation parameters, the deflection and maximum force of IPMC diaphragm were predicted in Chapter 4.

Table 2.2 Comparison of mean deformation of beam-shaped IPMC from experiment and simulation

Voltage (V)	Mean deformation (mm)		Error (%)	Force (mN)
	Experiment	Simulation		
1.5	6.25	6.32	1.18	0.63
3.0	26.75	28.91	7.08	2.92
5.0	29.25	29.00	−0.85	6.65

Chapter 3. Aerial Application: Glider Control Surface Actuation

3.1. Purpose of the Research

In this study, a glider was designed and fabricated. The mission scenario of the glider to perform was defined as follows:

① Glider drops freely without initial thrust

② While falling, control surface of the glider operates and changes the trajectory of the glider

③ Glider lands at the target point

④ Multiple control surfaces on the glider yields maneuverability of glider

In order to perform the scenario, this study aimed to configure an on-board system in which all of the components, including a power supply device, were placed. In order to design a light-weight glider, control surfaces of the glider were controlled using IPMC and paper was used for the glider body. The fabricated glider was verified through indoor drop test and the control surfaces actuated by IPMCs showed feasibility to control direction of the glider.

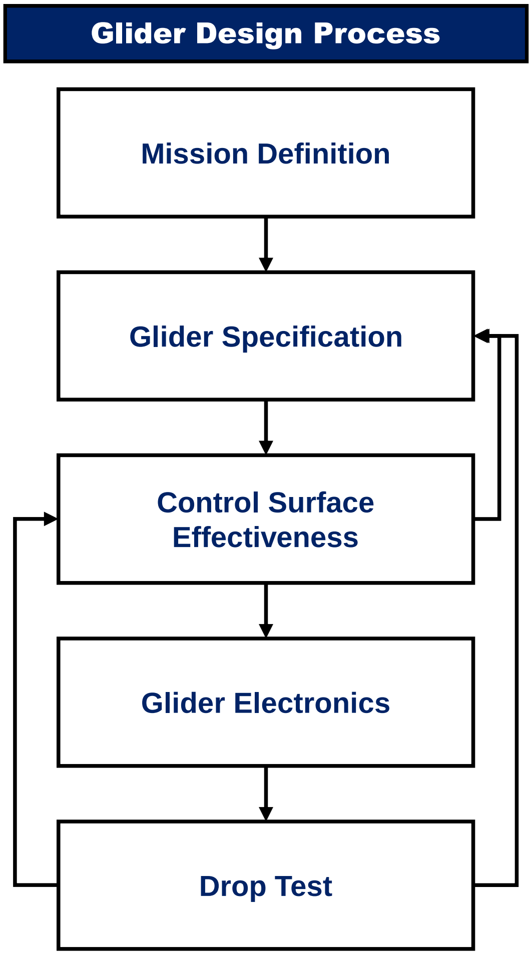

Figure 3.1 Design process for glider

The glider design process included following five steps as in Figure 3.1. As the mission for the glider was defined, glider specifications including glider weight, flight time, etc. were determined according to the designated mission. After the glider specifications were determined, control surface effectiveness, which shows whether the control surface sufficiently affects the flight, was calculated in order to design the control surface. Next, the glider electronics were designed, and finally the drop test with the fabricated glider was performed.

3.2. Glider and Control Surface Design

The glider developed in this study aimed to move in various direction after dropping without additional thrust. To guarantee the maneuverability of the glider, square-shaped glider with a control surface at each end was devised. The control surfaces were designed to control the direction of the glider drop by changing the vertical drag force of the glider. Therefore, it was necessary to design the control surface in conjunction with the shape of the glider.

3.2.1 Glider Specification

In order to determine the design of the glider, the following two conditions had to be satisfied:

① Flight time must be larger than 4 seconds in 15 m drop

② Glider must reach its terminal velocity with 15 m drop

By assuming 1-dimension fall with drag force, the glider's equation of motion was summarized as:

$$m\frac{dV}{dt}+\frac{1}{2}\rho C_D A V^2 - mg = 0 \qquad \text{Eq. 3.1}$$

Velocity V(t) and displacement x(t) according to time can be shown as follows:

$$V(t) = \sqrt{\frac{2mg}{\rho C_D A}} tanh\left(\sqrt{\frac{\rho C_D A g}{2m}} t\right), with\ initial\ velocity\ 0 \qquad \text{Eq. 3.2}$$

$$x(t) = \frac{2m}{\rho C_D A} ln\left(cosh\left(\sqrt{\frac{\rho C_D A g}{2m}} t\right)\right) \qquad \text{Eq. 3.3}$$

Figure 3.2 shows the flight velocity to time according to the glider projection area. The glider with area of 250 mm x 250 mm showed terminal velocity reached at 0.9 seconds, giving total flight time of 4.2 seconds in 15 m drop. Figure 3.3 shows allowable glider weight according to glider side dimension and flight time. Based on the calculations, a square-shaped glider design with a side length of 250 mm and a weight less than 0.1 kg was determined, and it is expected to have flight time longer than 4 seconds.

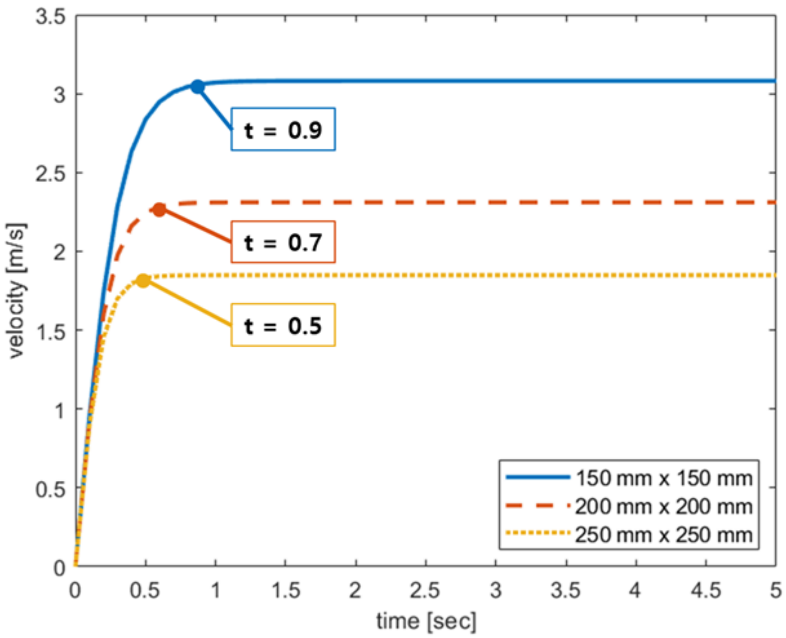

Figure 3.2 Velocity according to flight time of three different sizes of glider

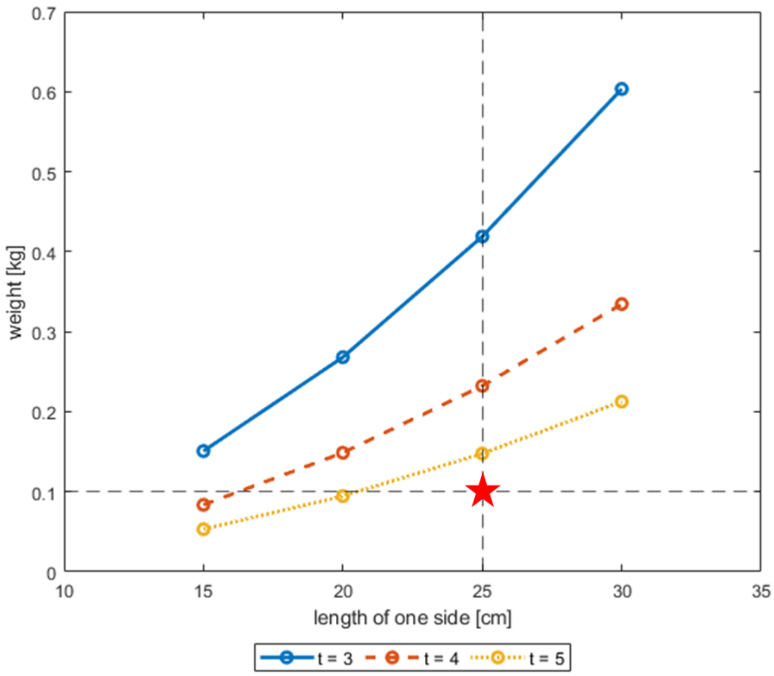

Figure 3.3 Side length limit of the glider which can carry 0.1 kg payload with more than 4 seconds flight time in 15 m drop

3.2.2. Control Surface Effectiveness

In this study, the gliding direction was affected by the change in orthogonal projection area. The orthogonal projection area could be changed by actuating flaps on the glider. Flaps were attached to each side of the square−shaped glider as shown in the Figure 3.4.

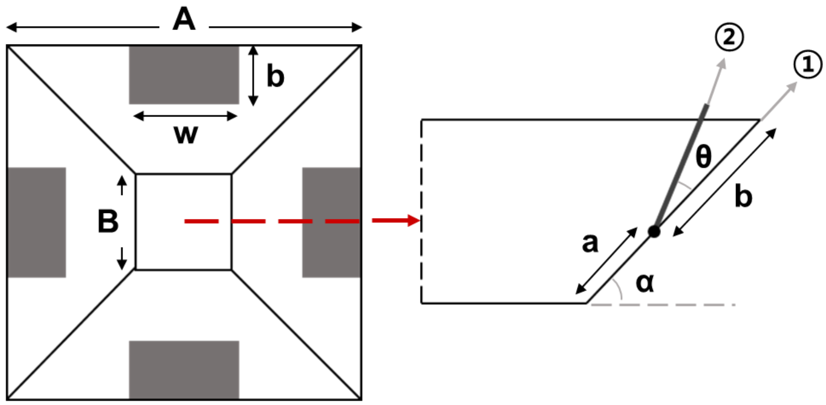

Figure 3.4 Glider dimension parameters

The change of the orthogonal area according to the flap angle θ was shown as:

Orthogonal area at ①:

$$S_1 = \frac{1}{2}(A+B) \times (a+b) \times cos\alpha \times 4 + B^2 \quad \text{Eq. 3.4}$$

Orthogonal area at ②:

$$S_2 = \frac{1}{2}(A+B) \times (a+b) \times cos\alpha \times 4 + B^2 - (w \times b) \times (cos\alpha - cos(\alpha+\theta)) \quad \text{Eq. 3.5}$$

Control surface effectiveness was defined as follows to determine dimensions and angle for each flap to change the direction of the glider during the falling period.

$$effectiveness = (1 - S_2/S_1) \times 100\ (\%) \qquad \text{Eq. 3.6}$$

Based on the control effectiveness, flap dimensions were determined as Table 3.1. Figure 3.5 shows control surface effectiveness according to the deflection flap angle at given flap dimensions. The plot shows effectiveness of 14.53% when the control surface is horizontal to the flight direction, $\theta > \pi/3$. This angle of the control surface had to be confirmed to be able to be reached by IPMC.

Table 3.1 Glider dimension parameters used in this study

A	250 mm
B	80 mm
w	70 mm
a	50 mm
b	50 mm
α	$\pi/6$ rad

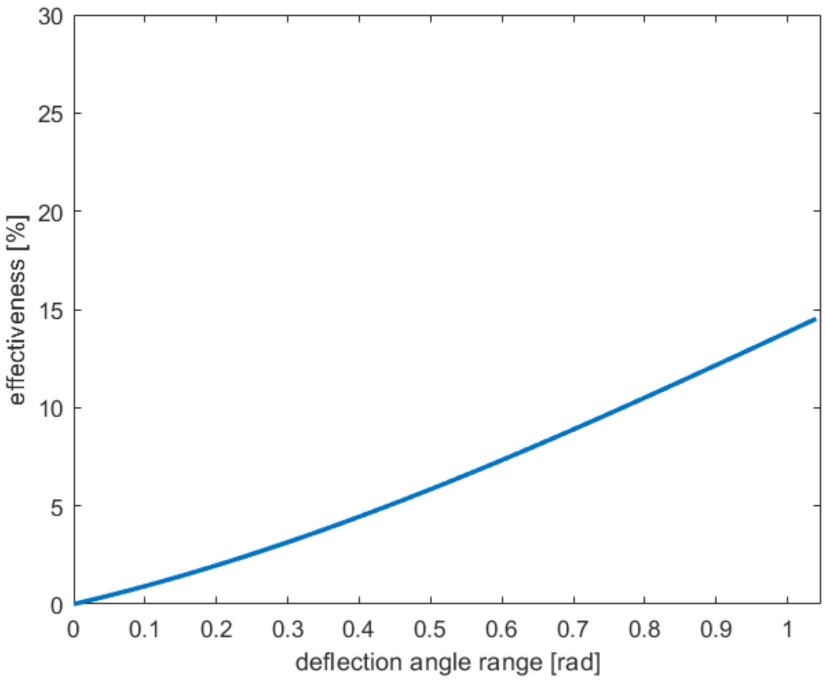

Figure 3.5 Glider control surface effectiveness plot showing effectiveness of 14.53% when fully activated

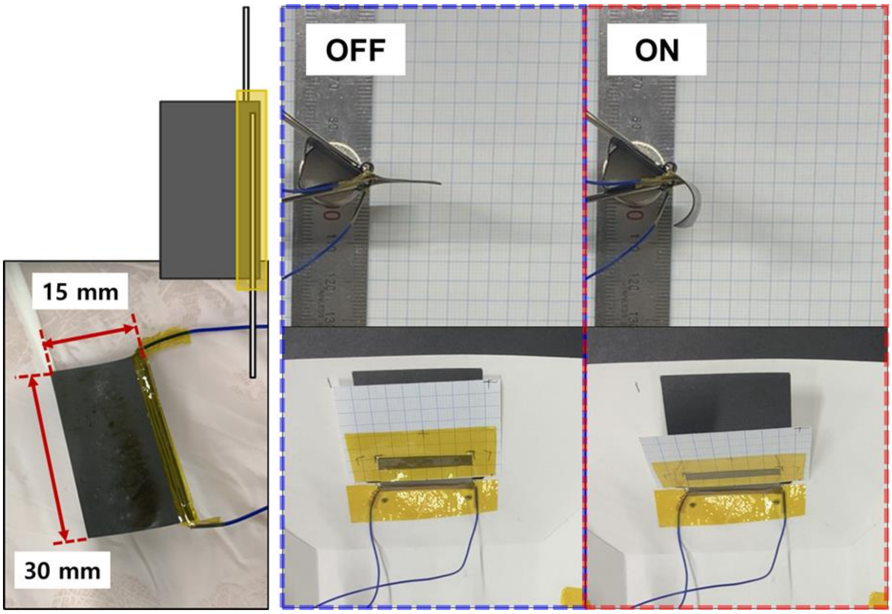

Figure 3.6 (Left) IPMC shape and packing method selected to actuate control surface, (right) IPMC actuation test to check actuation range and force

In order to successfully actuate the given size of glider control surface, hinge type IPMC was selected as shown in Figure 3.6. Dimension of the hinge type IPMC was decided to be 30 mm x 15 mm through actuation test. Actuation test was conducted to check whether the IPMC have enough actuation range and force to lift control surface of predetermined dimension.

3.2.3. Glider Electronics

In order to actuate glider control surfaces, glider electronics were developed. The glider electronics consist of 3 main components: MCU (Micro Controller Unit), Op-Amp and LiPo battery.

MCU performed real-time communication with ground control and controlled each control surface of the glider based on the received signals. Arduino Nano33 BLE was chosen as MCU. Op-Amp were used to amplify control signals from MCU, and being used as a switch, it applied the battery voltage to each IPMC. Two 3.7 V, 380 mAh LiPo batteries were used as the main power source for both MCU and IPMC.

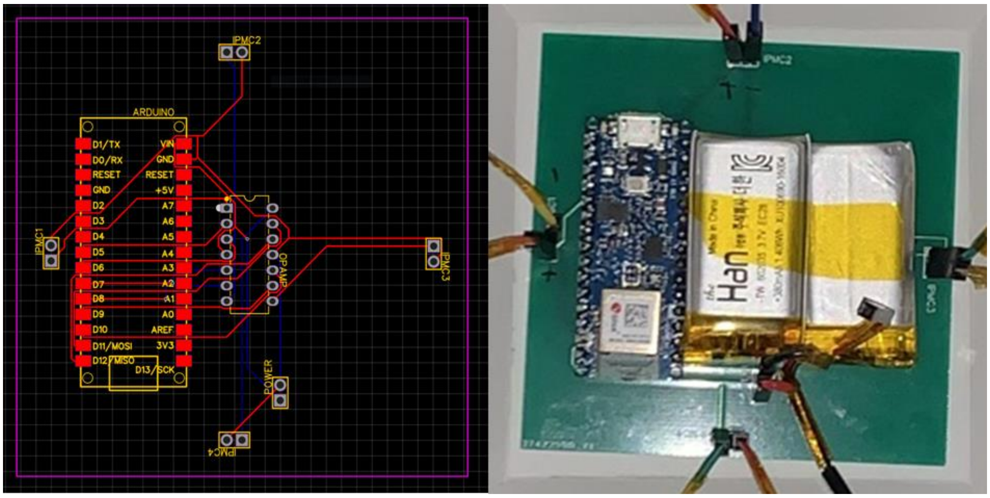

Figure 3.7 Glider electronics design and fabrication

3.3. Experimental Method

Finally, a square-shaped glider with 4 control surfaces was developed. The glider specifications are shown in Table 3.2. As determined in 3.2.1, overall weight including the glider body and the electronics was 45 g. The final glider is shown in Figure 3.8.

Table 3.2 Glider specifications

Size	(outer) 250 mm x 250 mm (inner) 80 mm x 80 mm
Weight	45 g
Material	(body) Drawing paper (flap) Wood-free paper (sealing) Kapton tape
Control surface	4-channel of 70 mm x 50 mm
Payload	MCU built-in gyroscope, accelerometer

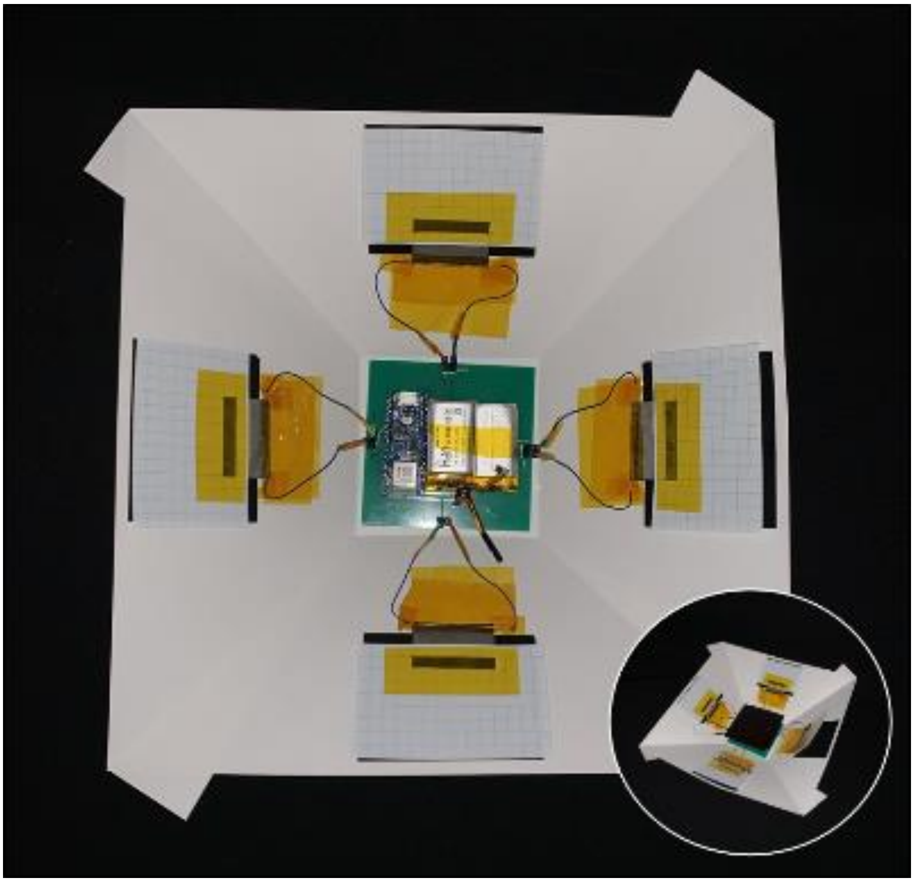

Figure 3.8 Fabricated glider, (circle) fabricated glider with sensor payload

The experiment was conducted to prove the feasibility of the glider. One channel of IPMC was remotely activated and dropped above 15m from the indoor ground. The drop was done within 5 seconds after activating the channel, at the constant fixed point. In order to prevent and minimize the impact of fabrication error, two identical gliders (Glider 1, Glider 2) were prepared. The experiment sequence was determined as follows:

① Glider 1, 2 activation check

② Glider 1: Activate channel 1 (Left), 2 times

③ Glider 1: Activate channel 3 (Right), 2 times

④ Glider 2: Activate channel 1 (Left), 2 times

⑤ Glider 2: Activate channel 3 (Right), 2 times

⑥ Glider 1: No activation, 2 times

⑦ Glider 2: No activation, 2 times

3.4. Results

3.4.1 Falling Behavior

As calculated in 3.2.1, all of the drop experiments were continued within 4 seconds. From the recorded video, unactuated control surfaces remained still, whereas actuated control surface was lifted. However, there was a rotational behavior shown at 80% of the entire dropping period. The rotational behavior caused 90° rotations from the initial orientation.

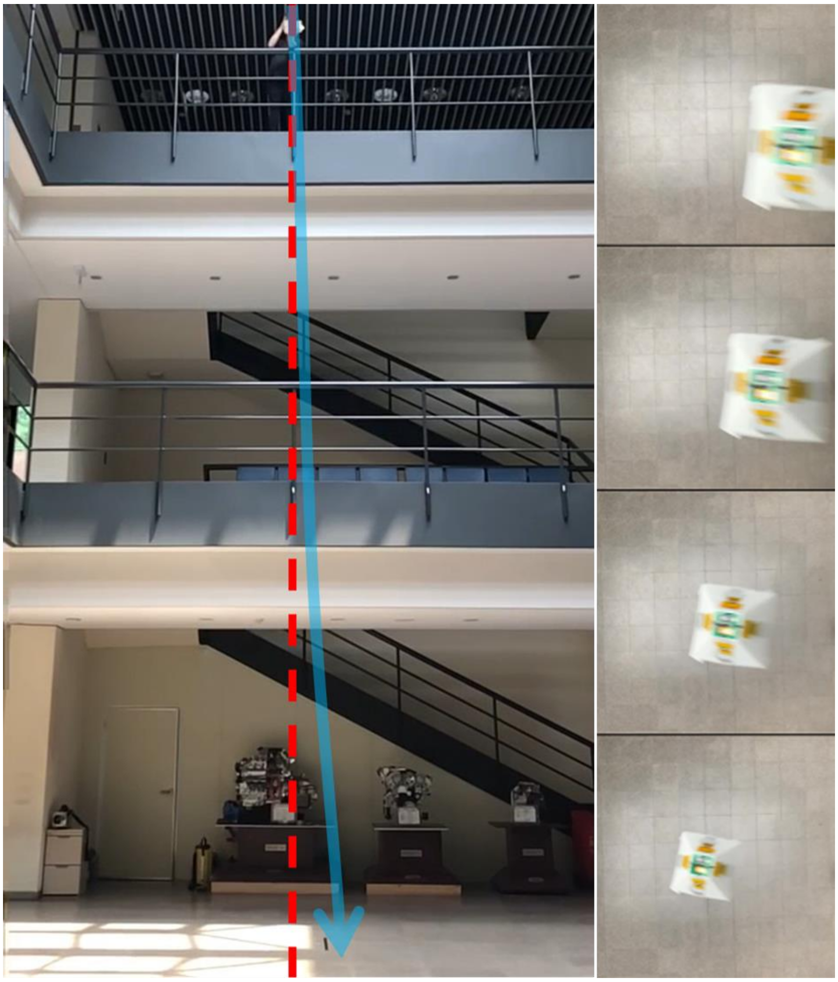

Figure 3.9 Glider falling behavior showing displacement change and rotation

3.4.2 Falling Position

The falling position of the gliders is shown in Figure 3.10. Both gliders consistently moved towards the actuated direction (i.e. glider with left control surface actuation moved to the left.). Y-axis variation was shown resulting from the rotational behavior. The maximum displacement was 250 mm from the drop position.

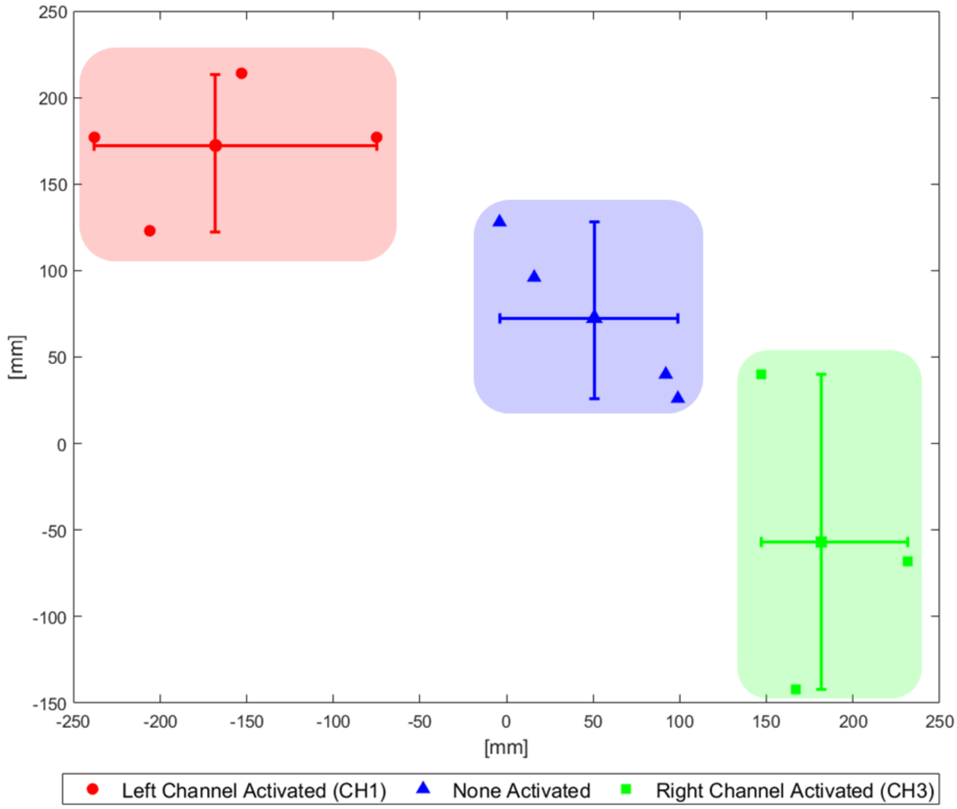

Figure 3.10 Glider drop test results showing successful actuation effectiveness

Chapter 4. Aquatic Application: Diaphragm Pump

4.1. Purpose of the Research

In this study, a pump that periodically discharges certain amount of liquid was designed and fabricated. In order to devise an effective pump, the diaphragm pumping method was selected. IPMC which can be driven with low voltage and actuated by its surface, was used to actuate the diaphragm. To discharge uniform amount of liquid, this study devised a method to reduce the hysteresis of IPMC. In addition, to effectively utilize IPMC to actuate diaphragm, IPMC shape was optimized to have the greatest deformation and tip force. Colored water was used as the target liquid.

4.2. Diaphragm Pump Design

Diaphragm pumping method discharges liquid by changing the pressure in the chamber through the vibration of the diaphragm. To this end, the design of IPMC was to be optimized through simulation, and the process of sealing the surface of IPMC was required to reduce hysteresis of the IPMC diaphragm and to ensure continuous and uniform pumping. A rough pump design was initially performed, and the shape of the IPMC was determined accordingly, and finally, the sealing method was determined.

4.2.1 Pump Design

The design of the pump is shown in the Figure 4.1. The pump consisted of reservoir, diaphragm chamber, and outlet.

Reservoir was where the liquid to be discharged is located. The liquid moved through the TFE tube located under the reservoir. The distance from the TFE tube to the upper surface of the reservoir was 30 mm, and the maximum pressure that the reservoir could exert on the liquid at atmospheric pressure was 0.2943 Pa.

The diaphragm chamber was where diaphragm is placed and actuated, which results in transferring the liquid. The liquid entering the chamber through the TFE tube moved to the outlet by the pressure change inside the chamber. The chamber had a shape of semi−sphere, with the maximum diameter of 20 mm. The depth of the chamber was 3 mm, which is the maximum deformation range of the diaphragm.

The reservoir to the outlet was connected through a TFE tube with outer diameter of 3.175 mm (1/8 inch) and internal diameter of 1.6 mm (0.063 inch). Liquid flowing through the tube was affected by the diaphragm by the slit in the tube in the diaphragm chamber. The entire tube was located on the same line without any change in height. The entire pump casing was manufactured by FDM 3D printing using ABS.

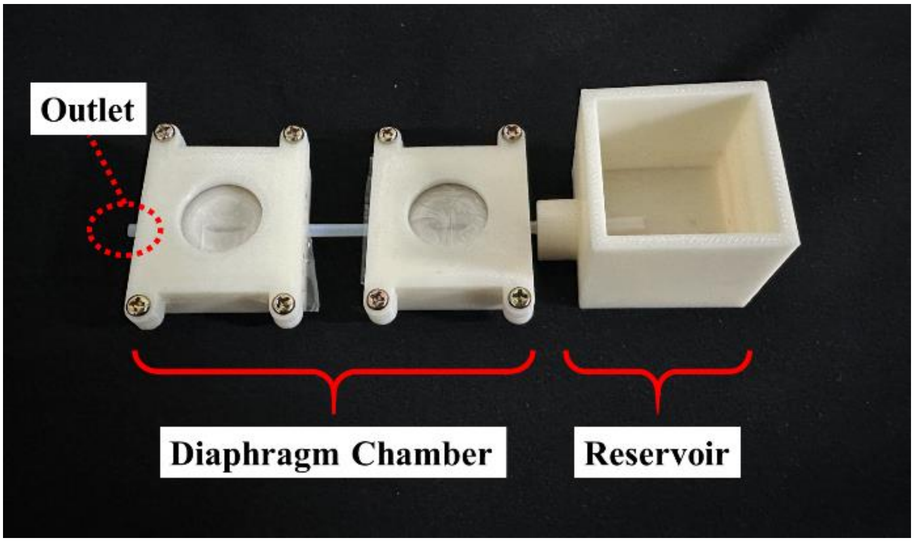

Figure 4.1 Diaphragm pump designed in this study

4.2.2 IPMC Design Optimization

Before fabricating the diaphragm using IPMC, the process of optimizing the shape of the diaphragm was performed using ANSYS simulations. The parameters used in Chapter 2.2 was applied in the simulation in order to predict the maximum deformations and tip forces of various IPMC shapes. The deformation under 50 seconds, constant 3 V was predicted using the properties shown in the Table 4.1.

In order to ensure the parameters in diaphragm shape of the IPMC, the results were matched with the real IPMC experiment. The deformation of IPMC diaphragm was measured with the LK−G30 laser displacement sensor with 250 Hz sampling rate.

Table 4.1 Specifications of IPMC used for diaphragm

Mass	0.69 g
Diameter	20 mm
Thickness	254 μm
E	132 MPa

Table 4.2 Comparison of mean deformation of diaphragm-shaped IPMC from experiment and simulation

Voltage (V)	Mean deformation (mm)		Error (%)	Force (mN)
	Experiment	Simulation		
1.5	0.217	0.560	158.3	2.60
3.0	0.609	0.877	43.9	11.85

Three types of IPMC shape was chosen as a candidate. The shape candidates are shown in Figure 4.2. Based on the simulation parameters obtained and used with the simulation, the maximum deflection and the tip force of each shapes were simulated. The simulation results for each type are shown in Table 4.3.

Through this method, IPMC diaphragm with a diameter of 20 mm and four bars (type 2 in Figure 4.2) were selected.

Table 4.3 Maximum deformation and maximum tip force of three different types of IPMC diaphragm shape

	Type 1	Type 2	Type 3
Max deformation (mm)	0.88	3.15	1.32
Tip force (mN)	11.85	14.75	33.00

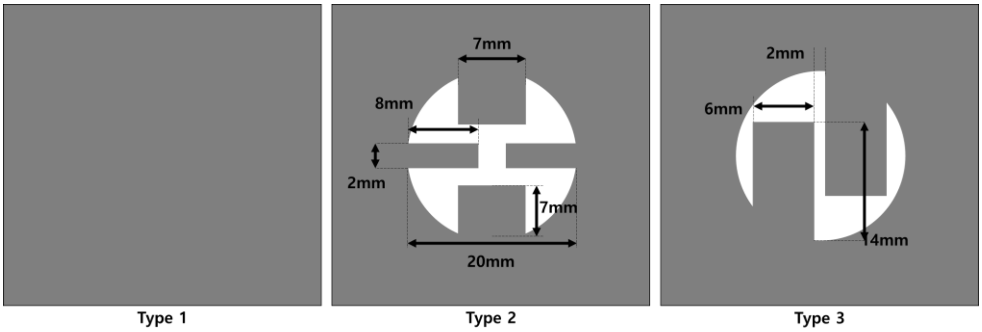

Figure 4.2 Three candidates of IPMC to actuate diaphragm

4.2.3 IPMC – Polyethylene Sealing

When IPMC is used without any sealing, since it actuates based on the surface moisture, high hysteresis occurs when moisture evaporates and results in great decrease in activation duration. To solve this problem, there have been previous researches packing IPMC to contact only one side of IPMC with the water or coating PDMS on the IPMC surface. However, such approaches limit usability of IPMC or often involves complicated and high−cost process. In addition, coating or sealing IPMC lowers maximum tip force and deflection of IPMC.

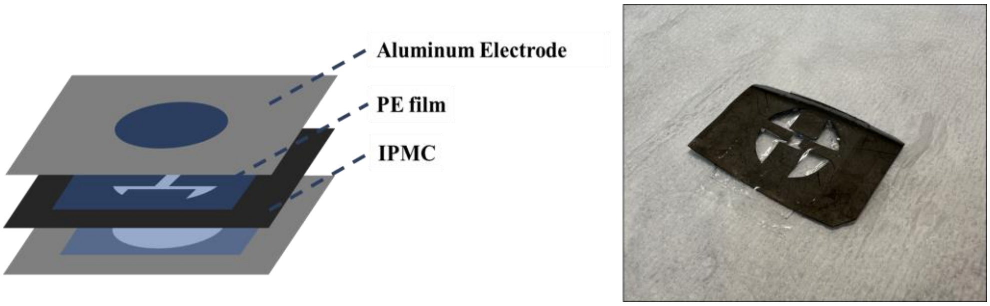

Figure 4 IPMC packing method and results

In this research, the activation part of IPMC was sealed using PE (Polyethylene) film with thickness of 12.7 μm, and the results were evaluated by measuring repeated deflection under 0.1 Hz, 3 V square voltage for 60 seconds. The experiment was conducted more than 3 times.

The result is shown in Table 4.4. Both IPMCs with and without PE sealing showed 6 peaks. The peak amplitudes were 3.71 times greater in IPMC without sealing. However, the amplitude greatly decreased as the time went on. For IPMC without PE sealing, the first and the last peak amplitude showed 2.59 times difference, where first peak amplitude was greater than the last. On the other hand, for IPMC with PE sealing, the first and the last peak amplitude showed 0.74 times difference.

This method of sealing IPMC with PE film was adopted in this study.

Table 4.4 Mean and standard deviation of peak amplitude of IPMC diaphragm with and without Polyethylene sealing

	Peak amplitude (mm)	
	Mean	Standard deviation
w/o PE	0.02802	0.01060
w/ PE	0.00755	0.00117
Comparison (%)	371	90.3

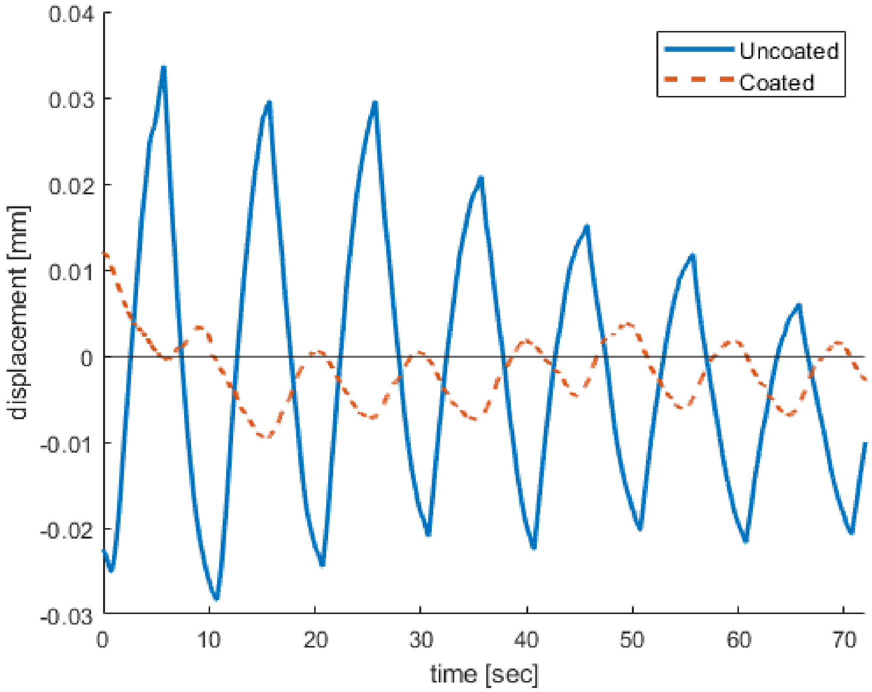

Figure 4.4 IPMC diaphragm hysteresis test showing more uniform peak values of sealed IPMC

4.3. Experimental Method and Results

The pump was assembled, and target liquid was set as colored water. Pump was actuated under square voltage of 3 V, 1/60 Hz, for 3 minutes. The discharged liquid was measured with the displacement of the liquid in TFE tube.

As a result, the pump could discharge constant 4.02 μL/min.

Chapter 5. Conclusions

In this study, IPMC was fabricated and the tip deformation and tip force were simulated and evaluated. The fabricated IPMC were utilized in two different environments.

5.1. Glider Control Surface Actuation

In aerial applications, a glider and control surfaces were designed to be activated by IPMC, using its light-weight and low driving voltage characteristic. The hinge-shaped IPMC was selected to lift the control surface as well as withstand the drag force in the direction of the gilder. The glider of less than 50 g was fabricated, and each control surfaces were remotely controlled. As a result, through a drop experiment, it was confirmed that the control surface of the glider could be effectively change the direction of the glider.

5.2. Diaphragm Pump

In aquatic applications, a diaphragm pump was designed to discharge uniform amount of liquid. By utilizing its surface actuation characteristic and biocompatibility, diaphragm was actuated by IPMC. Considering the low tip force of IPMC, optimization of the shape of IPMC was undergone to maximize the tip force of IPMC. High hysteresis was overcome by sealing the IPMC with polyethylene film.

As a result, the pump could discharge water with a flow rate of 4.02 μL/min.

Bibliography

(1) Hao, M., Wang, Y., Zhu, Z., He, Q., Zhu, D., and Luo, M. (2019). A Compact Review of IPMC as Soft Actuator and Sensor: Current Trends, Challenges, and Potential Solutions from Our Recent Work. *Frontiers in Robotics and AI,* 6. doi:10.3389/frobt.2019.00129.

(2) Bhandari, B., Lee, G., and Ahn, S.-H. (2012). A review on IPMC material as actuators and sensors: Fabrications, characteristics and applications. *International Journal of Precision Engineering and Manufacturing,* 13(1), 141-163, 2012. doi:10.1007/s12541-012-0020-8.

(3) Michel, S., Dürager, C., Zobel, M., and Fink, E. (2007). Electroactive polymers as a novel actuator technology for lighter-than-air vehicles. *Electroactive Polymer Actuators and Devices,* 65241Q. doi:10.1117/12.716658.

(4) Bian, C., Zhu, Z., Bai, W., and Chen, H. (2021). Highly efficient structure design of bending stacking actuators based on IPMC with large output force. *Smart Materials and Structures,* 30(7), 075033. doi: 10.1088/1361-665X/ac0398

(5) Lee, G., Choi, J., Kim, M., and Ahn, S.-H. (2011). Fabrication and reliable implementation of an Ionic polymer-metal composite (IPMC) biaxial bending actuator. *Smart Materials and Structures,* 20(10), 105026. doi:10.1088/0964-1726/20/10/105026.

(6) Sideris, E. A., De Lange, H. C., and Hunt, A. (2020). An ionic polymer metal composite (IPMC)-driven linear peristaltic microfluidic pump. *IEEE Robotics and Automation Letters,* 5(4), 6788-6795. doi:10.1109/lra.2020.3015452.

(7) Stemme, E., and Stemme, G. (1993). A valveless diffuser/nozzle-based

fluid pump. *Sensors and Actuators A: Physical,* 39(2), 159–167. doi:10.1016/0924-4247(93)80213-z.

(8) Fang, Y., and Tan, X. (2010). A novel diaphragm micropump actuated by conjugated polymer petals: Fabrication, modeling, and experimental results. *Sensors and Actuators A: Physical,* 158(1), 121–131. doi:10.1016/j.sna.2009.12.012.

(9) Nguyen, T. T., Goo, N. S., Nguyen, V. K., Yoo, Y., and Park, S. (2008). Design, fabrication, and experimental characterization of a flap valve IPMC micropump with a flexibly supported diaphragm. *Sensors and Actuators A: Physical,* 141(2), 640–648. doi:10.1016/j.sna. 2007.09.017.

(10) Wang, J., McDaid, A. J., Lu, C. Z., and Aw, K. C. (2017). A compact ionic polymer-metal composite (IPMC) actuated valveless pump for drug delivery. *IEEE/ASME Transactions on Mechatronics,* 22(1), 196–205. doi:10.1109/tmech.2016.2624762.

(11) Xu, B., Wang, S., Zhang, Z., Ling, J., and Wu, X. (2021). Improving the torsion performance of IPMC by changing the electrode separation. *Scientific Reports,* 11(1). doi:10.1038/s41598-021-87347-z.

(12) Lin, Y., Yu, C., Li, C., Liu, C., Chen, J., Chu, T., and Su, G. (2014). An Ionic-polymer-metallic composite actuator for reconfigurable antennas in mobile devices. *Sensors,* 14(1), 834–847. doi:10.3390/s140100834.

(13) He, C., Gu, Y., Zhang, J., Ma, L., Yan, M., Mou, J., and Ren, Y. (2022). Preparation and modification technology analysis of Ionic polymer-metal composites (ipmcs). *International Journal of Molecular Sciences,* 23(7), 3522. doi:10.3390/ijms23073522.

Abstract

본 연구는 폴리머 복합체의 일종인 IPMC (Ionic Polymer-Metal Composite, 이온성 폴리머 금속 복합체) 를 이용하여 기존의 모터 구동 시스템이 적용되기 힘든 시스템을 구동시키고자 하였다.

공중 환경에서는 글라이더의 제어 표면을 IPMC로 구동하였다. IPMC의 가벼운 특성과 저전압 구동이 가능한 특성은 본 적용에 사용되기 적합하였다. 이를 위하여 hinge-type의 IPMC를 선택하여 제어 표면을 구동시켰고, 제어 표면은 글라이더의 낙하 궤적을 효과적으로 변화시켰다.

수상 환경에서는 다이어프램 펌프를 IPMC로 구동하였다. IPMC의 생체적합성과 표면 구동 특성이 본 적용에 사용되기 적합하였다. 효과적인 적용을 위해 다이어프램을 구성하는 IPMC 형상을 힘을 극대화하는 방향으로 설계하였고, 구동의 히스테리시스를 감소시킬 수 있는 실링 방법을 개발하였다.

각 적용에서 IPMC를 효율적으로 적용하기 위해 적절한 구동 방법과 패키징 방법이 개발되었다.

주요어: 이온성 폴리머-금속 복합체 구동기, 제어 표면, 다이어프램 펌프

학번: 2021-28477